#### ORIGINAL PAPER



# Nonreciprocal and directional wave propagation in a two-dimensional lattice with bilinear properties

Zhaocheng Lu

· Andrew N. Norris

Received: 21 May 2021 / Accepted: 3 September 2021 / Published online: 26 September 2021 © The Author(s), under exclusive licence to Springer Nature B.V. 2021

**Abstract** A passive method of realizing nonreciprocal wave propagation in a two-dimensional (2D) lattice is proposed, using bilinear springs combined with the necessary spatial asymmetry to provide a stable and strong departure from reciprocity. The bilinear property is unique among nonlinear mechanisms in that it is independent of amplitude but sensitive to the sign of the wave motion; the 2D setup allows the flexibility of generating spatial asymmetry at both small and large scales. The starting point is a linear 2D monatomic spring-mass lattice with strong directionally dependent wave propagation. The source and receiver are aligned so that there is virtually no direct wave transmission between them. Adding a region of bilinearity combined with spatial asymmetry that is not in the direct path between the source and receiver causes signal transmission via nonreciprocal scattering. A variety of spatially asymmetric bilinear configurations are considered, ranging from compact modulations confined within the unit cell to extended ones over the whole section, to obtain different dynamic nonreciprocal effects. Simulations illustrate how the combination of bilinearity and spatial asymmetry ensures a passive amplitude-independent nonreciprocal 2D system for a variety of different excitations.

**Keywords** Nonreciprocity · Bilinear stiffness · 2D Lattice · Directional propagation · Spatial asymmetry · Amplitude independence · Passive method

#### 1 Introduction

Reciprocity is a fundamental physical principle of wave motion that guarantees symmetric wave transmission between a source and a receiver. Interchanging the positions of source and receiver in a reciprocal medium results in the same signal. Overcoming this restriction can lead to comprehensive control of wave propagation [1]. Breaking reciprocity in one-dimensional (1D) structures can be achieved in many different ways, either using external energy to modulate the system properties (active methods) or introducing nonlinearity with spatial asymmetry (passive methods). The energetic approaches fall into two types of methods: introducing moving parts or circulating flows in the propagation medium [2,3] and performing spatial-temporal modulations of the system properties [4–10]. The passive methods typically make use of various nonlinear mechanical properties and the necessary ingredient of spatial asymmetry [11–17]. Many researchers have successfully realized breaking reciprocity in 1D domain via active and passive approaches, demonstrating effects such as one-way acoustic and elastic wave propagation [1,4-8,15,16,18], asymmetric energy transfer [1, 10, 13, 17] and nonreciprocal phase shift [1,3].

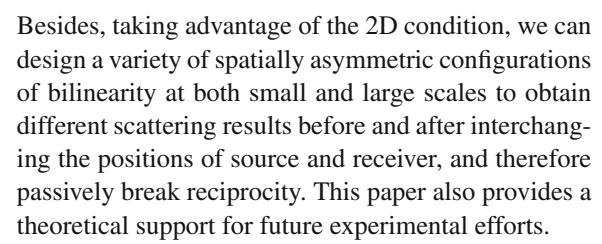
(⊠)Z. Lu · A. N. Norris

Department of Mechanical and Aerospace Engineering, Rutgers University, Piscataway, NJ 08854-8058, USA Z. Lu: e-mail: zhaocheng.lu@rutgers.edu



However, in 2D space only the active nonreciprocal systems have been considered. Of the two principle methods used, the first is nonreciprocal topologically protected edge states (TPESs) that appear at the interface between two topologically inequivalent insulators. For nonreciprocal TPESs, unidirectional wave propagation along an interface is supported because one of the two topologies is created by breaking time-reversal symmetry. Active components, which are able to modulate the physical properties in time, are typically used to break time-reversal symmetry. Examples are experimentally realized lattices of gyroscopes [19], lattices of acoustic circulators with moving fluid involved [20] and theoretical studies of chiral edge modes in hexagonal and square gyroscopic lattices [21]. The second active method uses space-time modulation, as in 1D. For example, nonreciprocal transmission of Rayleigh surface waves with one-way mode conversion can be realized in a continuous 2D semi-infinite medium bound with an array of space-time modulated springmass oscillators [22]. Both the topological insulators and the semi-infinite medium with complex interface are active nonreciprocal systems which require external energy input, and as a consequence, they are potentially unstable.

Here, we concentrate on a passive approach to breaking wave reciprocity in a specific 2D system. We take advantage of the fact that 2D periodic structures usually exhibit directional wave propagation when some requirements, e.g., structural properties and wave frequency range, are satisfied [23–25]. This phenomenon indicates the existence of propagation-free region in those structures, which inspires us to come up with a strategy of realizing the customized nonreciprocal behavior: wave transmission in the propagation-free region with opposite signs of displacements. Material nonlinearity combined with spatial asymmetry can be added to the 2D periodic structure, redirecting the signals to a propagation-free region via scattering from the asymmetric nonlinear section. Similar idea is found in some previous works, where cubic nonlinearity has been used in 2D lattices to introduce tunable wave directionality [24,25]. However, these systems are heavily dependent on excitation amplitude and are still reciprocal because of the lack of the necessary and essential ingredient of spatial asymmetry for breaking reciprocity. Instead, we use bilinearity, which is independent of amplitude but sensitive to the sign of wave motion, to generate a stable and strong nonlinearity.



The outline of the paper is as follows. Section 2 discusses the physical structure of the linear 2D monatomic lattice and the directional wave propagation properties. The design principle of breaking reciprocity by adding a bilinear section with spatial asymmetry to the lattice is introduced in Sect. 3. Based on the flexibility of generating spatial asymmetry in the 2D lattice, we start with micro-modulations within each unit cell of the bilinear section in Sect. 4. Interpretation and amplitude independence of the nonreciprocal effect are demonstrated, and several simulation arrangements are considered. An additional design approach using macro-modulations of the whole bilinear section in its entirety is then discussed in Sect. 5. Section 6 concludes the paper.

#### 2 2D Monatomic lattice

#### 2.1 Equations of motion

A 2D monatomic lattice is modeled as an array of equal masses interconnected by shear springs, as shown in Fig. 1. Transverse (into- and out-of-plane) displacement is the single degree of freedom describing the motion of each mass, and springs are assumed to act in shear with a force related to the relative displacement of neighboring masses. The unit cell therefore consists of a block with mass and a mass-less "+" shape structure (no force between them) with thickness, width and length  $d \rightarrow 0$  as Fig. 1 shows. The length-less "+" shape structure is able to transfer force between neighboring masses, leading to the transverse wave propagation while neglecting rotational motion. Two states ("+" shape up and down) exist in this 2D lattice, guaranteeing the spatial symmetry of the lattice.

The periodicity of the lattice is defined by orthogonal lattice vectors  $a_1\vec{i}_1$  and  $a_2\vec{i}_2$  in the horizontal and vertical direction, respectively. The mass at location  $n_1 a_1\vec{i}_1 + n_2 a_2\vec{i}_2$ , shown in gray box at the center in Fig. 1(c), satisfies the equilibrium equation (supposing that the forces exerted by the shear springs are much



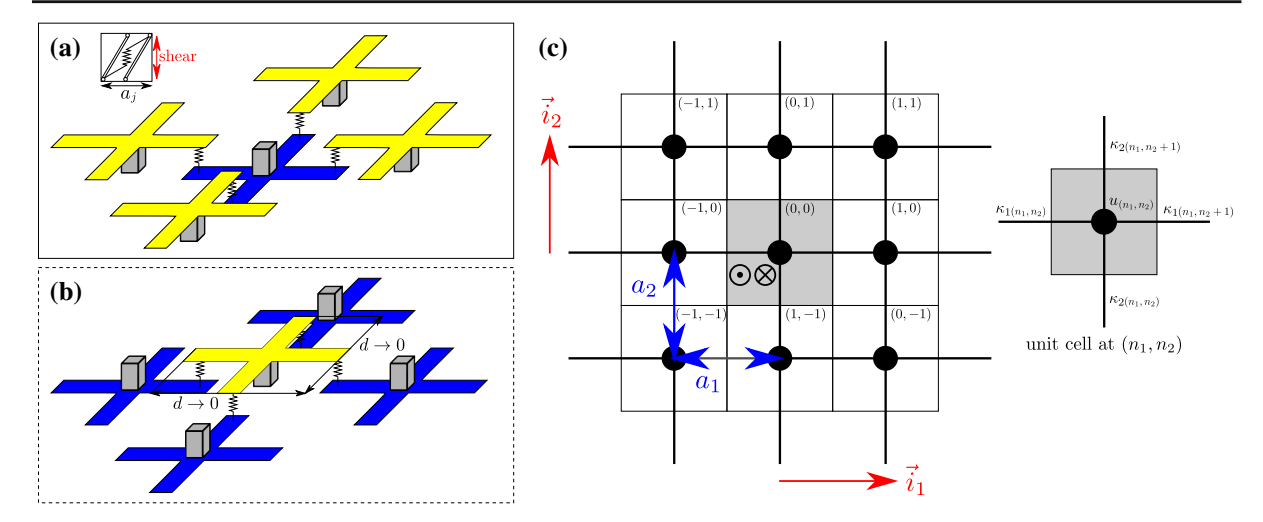


Fig. 1 2D monatomic lattice of identical masses connected by shear springs.  $\bf a$  and  $\bf b$  depict the physical structure of a unit cell and four neighboring unit cells in the monatomic lattice; the unit cell consists of a block with mass and a mass-less "+" shape structure of size  $d \to 0$  introducing the in-plane transverse wave propagation; and  $\bf a$  stands for the state of "+" shape up and  $\bf b$  down. The insert in  $\bf a$  is a schematic of a shear spring

with structural length  $a_j$ , j=1,2.  ${\bf c}$  shows the reference system; the mass displacement is in the transverse direction (into-and out-of-plane) only. In order to eliminate reflections from the boundaries for numerical simulations, the finite lattice is surrounded by perfectly matched layers (PMLs), see Appendix A for details

greater than gravity and neglecting rotational motion)

$$m \ddot{u}_{(n_1, n_2)} = \sum_{j=1}^{2} \left[ \kappa_j^- \Delta u_j^- + \kappa_j^+ \Delta u_j^+ \right], \tag{1}$$

where

$$\kappa_{i}^{-} = \kappa_{j (n_{1}, n_{2})}, \ \kappa_{i}^{+} = \kappa_{j (n_{1} + \delta_{j1}, n_{2} + \delta_{j2})},$$
(2)

with j = 1 and 2 denoting stiffnesses of the springs located along the horizontal and vertical direction, respectively, and

$$\Delta u_{j}^{\pm} = u_{(n_{1} \pm \delta_{j1}, n_{2} \pm \delta_{j2})} - u_{(n_{1}, n_{2})}, \qquad (3)$$

representing the relative transverse displacement of two adjacent masses.

#### 2.2 Wave directivity of a linear lattice

The dispersion relation between the frequency  $\omega$  and the wave vector  $\vec{k} = k_1 \vec{i}_1 + k_2 \vec{i}_2$  plays an important role in deciding the wave propagation in the lattice. Setting the transverse displacement of the neighboring masses as

$$u_{(n_1\pm 1, n_2\pm 1)} = u_{(n_1, n_2)} e^{i(\pm k_1 a_1 \pm k_2 a_2)}$$
(4)

and assuming time dependence  $e^{-i\omega t}$  yield the dispersion relation

$$\omega^2 = \frac{2}{m} \left[ \kappa_1 \left( 1 - \cos k_1 a_1 \right) + \kappa_2 \left( 1 - \cos k_2 a_2 \right) \right]. \tag{5}$$

Based on Eq. (5), we plot the dispersion surface and the corresponding isofrequency contours for the monatomic lattice in Fig. 2a and b.

The group velocity

$$\vec{c}_g = \frac{\partial \omega}{\partial k_1} \vec{i}_1 + \frac{\partial \omega}{\partial k_2} \vec{i}_2 \equiv c_{g1} \vec{i}_1 + c_{g2} \vec{i}_2, \tag{6}$$

where

$$c_{gj} = \frac{a_j \kappa_j}{m\omega} \sin k_j a_j \,, \quad j = 1, 2, \tag{7}$$

is depicted in Fig. 2c; note that the contour is closed only for the case of wave propagation in all directions.

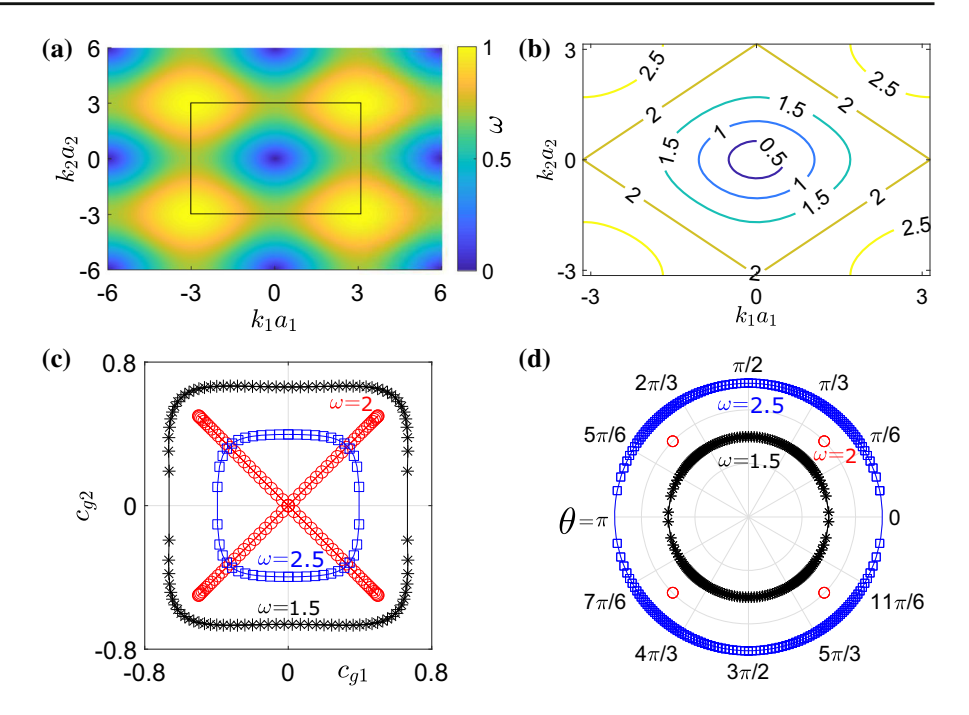
The angle formed between normal to the isofrequency contour and the horizontal axis in Fig. 2b is denoted as  $\theta$ , which defines the direction of wave energy propagation at the corresponding frequency and wavenumber pair. The propagation directions are shown in the polar plot in Fig. 2d, and the expression of propagating angle following from Eq. (7) is

$$\theta = \tan^{-1} \frac{a_2 \kappa_2 \sin k_2 a_2}{a_1 \kappa_1 \sin k_1 a_1}, \tag{8}$$

where the values of  $k_1$  and  $k_2$  are specified by the isofrequency contour of Fig. 2b for a selected frequency  $\omega$ .



Fig. 2 Tools for the analysis of wave directivity. a Dispersion surface. b Isofrequency contours of frequency distribution within the first Brillouin zone (black rectangle) in (a);  $\theta$  defines the direction of wave energy propagation. c Group velocity (50 data points per plot). d Directions of wave energy propagation (200 data points per plot). Here,  $a_1 = a_2 = 1$  $m, \kappa_1 = \kappa_2 = 1 \text{ N/m},$ m=1 kg, and frequency  $\omega$ is measured in rad/s



#### 3 Design of nonreciprocal 2D monatomic lattice

The design for breaking reciprocity takes advantage of the directional nature of wave propagation in the 2D lattice. The idea, illustrated in Fig. 3, is as follows. In the linear case, directional wave propagation from source in Fig. 3a cannot be detected at receiver (A  $\rightarrow$  B or B  $\rightarrow$  A) because the latter is, by choice, located in a propagation-free region relative to the source. Then, by introducing bilinearity with spatial asymmetry in a place that a wave can reach from the source, see Fig. 3b, a signal will travel from the source to the receiver via scattering from the bilinear section. A different response will be observed after interchanging the positions of source and receiver, see Fig. 3c, due to non-reciprocity achieved by the combination of bilinearity and spatial asymmetry.

Spatial asymmetry is a necessary ingredient for breaking reciprocity passively in a bilinear medium. Given the 2D condition, we have the flexibility of combining bilinearity with various spatially asymmetric setups. Here, we start with the modulations confined within each unit cell of the bilinear section, achieving the asymmetric arrangements in the microscopic manner. Then, we apply the additional modulations of asymmetry to the whole bilinear section as its entirety from the macro-perspective.

### 4 Micro-modulation: spatial asymmetry of unit

The system remains reciprocal despite the bilinearity introduced if it is spatially symmetric. Here, we discuss different ways of introducing microstructural spatial asymmetry within the unit cell of nonlinear section and therefore breaking reciprocity.

#### 4.1 Stiffness and structural asymmetry

To start with, spatial symmetry for a unit cell of a linear 2D monatomic lattice indicates that the same resultant shear force,  $F_j^{\pm} = \kappa_j^{\pm} \Delta u_j^{\pm}$ , can be obtained given the identical relative displacement between the unit cell and its nearest neighbors,  $\Delta u_j^{\pm}$ ,

$$\begin{cases} \Delta u_j^- = \Delta u_j^+ \\ \kappa_j^- = \kappa_j^+ \end{cases} \Rightarrow F_j^- = F_j^+, \tag{9}$$

j=1 when we consider the neighboring unit cells in horizontal direction, and j=2 in vertical direction.

Spatial symmetry still holds in the unit cell when all linear springs are replaced by the identical bilinear springs (labeled by  $\nearrow$  and the corresponding stiffness written as  $\kappa_{\nearrow}$ ) as shown in Fig. 4a. Although the bilinear spring has different stiffnesses when it is compressed and stretched, two horizontally or vertically



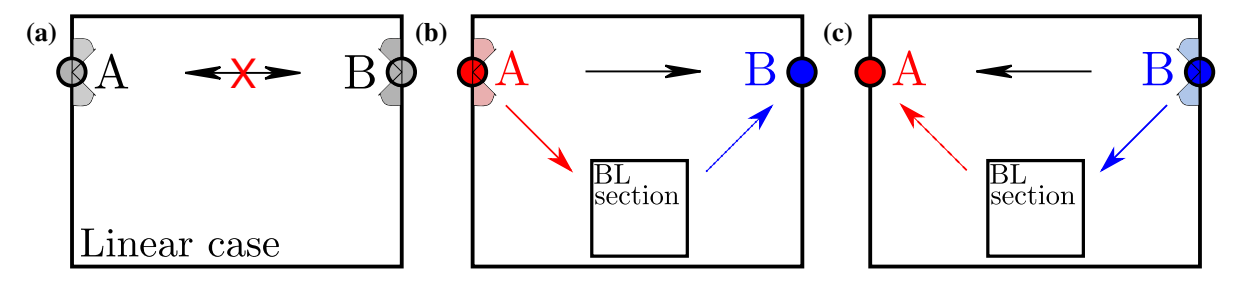


**Fig. 3** Schematic diagram of the design for a nonreciprocal 2D monatomic lattice. **a** depicts directionally limited wave propagation in the linear lattice, where the propagating range is indicated by shaded angles; receiver at B (A) is located in the propagation-free region relative to source at A (B). The bilinear section (square box) combined with spatial asymmetry is then introduced in a

place that a wave can reach from the source;  $\mathbf{b}$  and  $\mathbf{c}$  illustrate that a signal will travel from the source to the receiver via scattering from the asymmetric bilinear section, and interchanging the positions of source and receiver results in different responses because of the spatial asymmetry in the bilinear region (not shown)

**Table 1** Stiffness properties of bilinear springs.  $\kappa$  is the linear stiffness, and  $\Delta \kappa_{\pm}$  are the deviations from linear stiffness. By current setting, we get  $\kappa_{(c \text{ or } t)/} \neq \kappa_{(c \text{ or } t)}$ , or more specifically,  $\kappa_{(c \text{ or } t)/} = \kappa_{(t \text{ or } c)/}$ 

Bilinear Spring Label	Comp. Stiff.	Tens. Stiff.
7	$\kappa_{c} \nearrow = \kappa - \Delta \kappa_{-}$	$\kappa_{t} \nearrow = \kappa + \Delta \kappa_{+}$
$\searrow$	$ \kappa_{c} = \kappa + \Delta \kappa_{+} $	$ \kappa_t \leq \kappa - \Delta \kappa $

adjacent bilinear springs are always in the same condition given the identical relative displacement, such that

$$\begin{cases} \Delta u_j^- = \Delta u_j^+ \\ \kappa_i^- = \kappa_j^+ \equiv \kappa_{(c \text{ or } t)} \end{cases} \Rightarrow F_j^- = F_j^+, \tag{10}$$

where  $\kappa_{c\nearrow}$  stands for the compressive stiffness of the bilinear spring labeled by  $\nearrow$  and  $\kappa_{t\nearrow}$  the tensile stiffness.

One way to generate spatial asymmetry within the unit cell is to modify the stiffness property of the bilinear springs in an alternating manner. In Fig. 4c, we replace the bilinear spring on the right of  $\nearrow$  label with that of  $\searrow$  label (therefore, we have j=1 for the following relevant equations, representing the replacement in the horizontal direction); these two springs exhibit different stiffnesses when compressed and stretched, see Table 1. This modulation generates different resultant shear forces despite given the same relative displacement between the unit cell and its nearest neighbors, i.e.,

$$\begin{cases} \Delta u_1^- = \Delta u_1^+ \\ \kappa_1^- \equiv \kappa_{(c \text{ or } t)} \nearrow \neq \kappa_1^+ \equiv \kappa_{(c \text{ or } t)} \searrow \end{cases} \Rightarrow F_1^- \neq F_1^+.$$

$$\tag{11}$$

The alternative micro-modulation is depicted in Fig. 4e. One leg in "+" shape structure of the unit cell is moved to the opposite position, up or down. Without modifying any bilinear spring, the asymmetric structure results in the opposite conditions for two adjacent bilinear springs in horizontal direction (j=1) given the same relative displacement. Consequently, one compressed bilinear spring and the other stretched one can exert the different resultant shear forces,

$$\begin{cases} \Delta u_1^- = \Delta u_1^+ \\ \kappa_1^- \equiv \kappa_{(c \text{ or } t)} \nearrow \neq \kappa_1^+ \equiv \kappa_{(t \text{ or } c)} \nearrow \end{cases} \Rightarrow F_1^- \neq F_1^+.$$

$$\tag{12}$$

Considering the setup of  $\kappa_{(c \text{ or } t)\nearrow} = \kappa_{(t \text{ or } c)\searrow}$ , see Table 1, two introduced methods of generating spatial asymmetry within the unit cell are functionally identical.

From the perspective of horizontal chain, the spring condition and resultant shear force for the symmetric and asymmetric (reciprocal and nonreciprocal) unit cell are self-evident, see Fig. 4b, d and f. In reciprocal case, as shown in Fig. 4b, for any two adjacent bilinear springs, the identical relative displacement leads to the same spring condition and the same resultant shear force. For our first strategy of generating spatial asymmetry shown in Fig. 4d, the bilinear springs are reversed alternately; even though the identical relative displacement results in the same condition for the adjacent reversal bilinear springs, different resultant shear



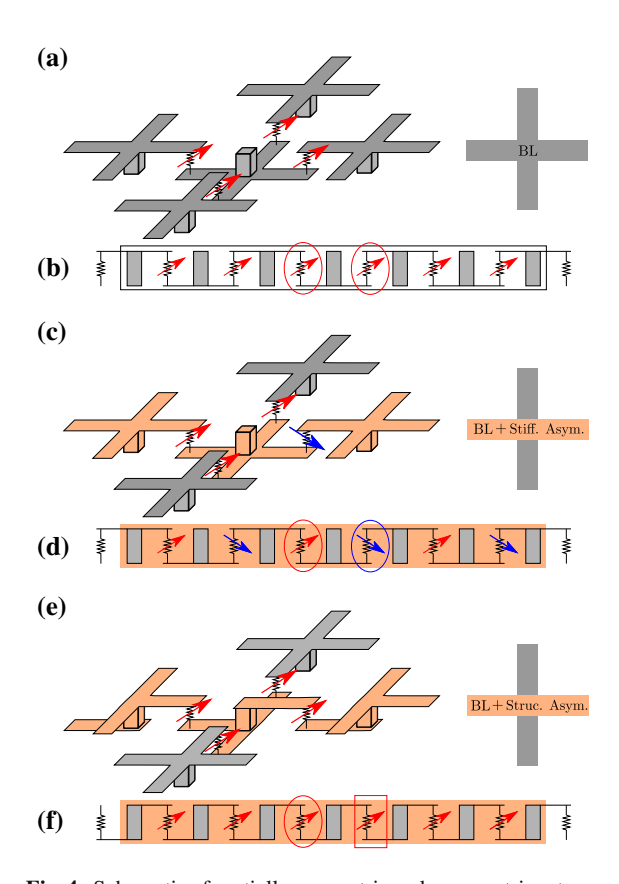


**Fig. 4** Schematic of spatially symmetric and asymmetric setups. **a** shows the physical structure of a unit cell in the bilinear section connecting its nearest neighbors by identical bilinear springs, but without spatial asymmetry. **c** and **e** are two functionally identical asymmetric setups, with the asymmetric modulation in horizontal direction only. The shaded bars on the right illustrate the spatially symmetric or asymmetric conditions in corresponding directions. We alternate the bilinear spring connected to the unit cell in (**c**), leading to bilinear *stiffness asymmetry*; in (**e**), one leg in "+" shape structure is moved to the opposite position, resulting in *structural asymmetry* of the unit cell. **b**, **d** and **f** depict the horizontal chains of unit cells with corresponding bilinear setups, which intuitively show the compressive/stretched conditions of the bilinear springs and assist in the analysis of spatially asymmetric systems

forces are obtained. The structural asymmetry can be achieved using the second strategy as shown in Fig. 4f; the same relative displacement results in the opposite conditions for two adjacent identical bilinear springs and therefore different resultant shear forces.



#### 4.2 Numerical experiments

From now on, let us discuss the numerical simulations of wave propagation in the 2D monatomic lattice. To generate incident wave, a continuous displacement restriction is applied to source position,

$$u = \mathcal{H}(t) U \sin \omega t \,, \tag{13}$$

where U is input amplitude,  $\omega$  is the excitation frequency, and  $\mathcal{H}$  represents the Heaviside function. The positions A and B, which are used to locate the source and receiver, are aligned so that there is virtually no direct wave transmission between them when strong directionally dependent wave propagates.

Assuming that  $a_1 = a_2 = 1$  m,  $\kappa_1 = \kappa_2 = 1$  N/m, m = 1 kg for model setup, and U = 1 m,  $\omega = 2$  rad/s for excitation, we can obtain directional wave propagation in four discrete directions with angle  $\theta = \frac{n\pi}{4}$ , n = 1, 3, 5, 7, refer to Fig. 2c and d. Simulation result of this directional wave propagation in a pure linear lattice is shown in Fig. 5a.

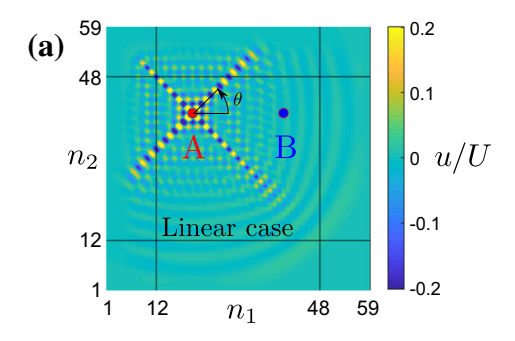
The location of an introduced bilinear section is then chosen so that the mentioned directional propagating wave can reach it. We take the bilinear section as a square with  $2N \times 2N$  bilinear springs, see Fig. 5b, whose center at angle  $\theta = -\frac{\pi}{4}$  relative to the position A and  $\theta = \frac{5\pi}{4}$  for B. Therefore, the positions A and B are equally distant by  $N_0$  springs from the center of the bilinear section.

Here, we set the number of springs  $N_0 = 10$  specifying the source and receiver positions, and N = 8 defining the bilinear section size. Extreme bilinearity guarantees the significantly nonreciprocal results, requiring drastic difference between tensile and compressive stiffness, e.g.,  $\Delta \kappa_- \ll \Delta \kappa_+$ , see Table 2 for details of stiffnesses selection.

#### 4.3 Nonreciprocity

Three different setups are tested, and the simulation results illustrate that combination of bilinearity and spatial asymmetry is able to break reciprocity.

Case 1: Pure linear. A pure linear setup is shown in Fig. 6a, and the resultant dynamic profiles at the receivers are in Fig. 6b. The overlapping low-amplitude results observed before and after interchanging the positions of source and receiver, typically below 10% of the excitation amplitude, not only indicate that the



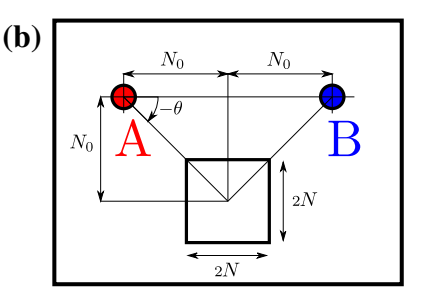


**Fig. 5** Incident wave and simulation setup. (a) shows the incident wave directionally propagating with angle  $\theta$  in a pure linear lattice, generated by a continuous excitation, see Eq. (13). (b) illustrates the bilinear section, assumed to be square with sides

of 2N bilinear springs in length; the positions A and B (used to place the source and receiver) are equally distant from the center of the bilinear section with  $N_0$  springs in both horizontal and vertical directions

**Table 2** The stiffness of linear and bilinear springs. All linear springs are identical. The expressions of bilinear springs can be found in Table 1 with  $\kappa_{c, 7} \ll \kappa_{t, 7}$ ,  $\kappa_{c, \searrow} \gg \kappa_{t, \searrow}$  and  $\kappa_{(c \text{ or } t), 7} = \kappa_{(t \text{ or } c), \searrow}$ . The unit of stiffness in this table is N/m

$ \kappa_1 = \kappa_2 = \kappa $	$\Delta \kappa$	$\Delta \kappa_+$	$\kappa_{c}$ 7	$\kappa_{t}$ /	$\kappa_{c\searrow}$	$\kappa_{t}$
1	0.875	10	0.125	11	11	0.125

receivers are located at the propagation-free zone relative to the sources but illustrate the reciprocity.

Case 2: Bilinearity only. In Fig. 6c, we introduce a nonlinear section with bilinearity in both horizontal and vertical directions to the place where directional wave propagation can reach, refer to Fig. 5b. However, the overlapping low-amplitude dynamic profiles in Fig. 6d indicate that a bilinear section without spatial asymmetry cannot break reciprocity.

Case 3: Bilinearity + spatial asymmetry. We combine the bilinearity with spatial asymmetry and arrange this combination along the horizontal direction only within the bilinear section (the vertical direction remains solely bilinear) as shown in Fig. 6e. The resultant dynamic profiles have the opposite shifts in Fig. 6f: A positive shift is obtained when the incidence comes from position A, and that from B gives a negative shift. Even though the normalized amplitude is still relatively low, roughly between 30 and 60%, we lay more emphasis on the nonreciprocal dynamic behaviors with steady opposite shifts.

#### 4.4 Interpretation of nonreciprocal effects

The reason for the opposite signs in dynamic profiles is discussed. Based on our previous explorations in the

1D bilinear spring—mass chain system [15], we conclude that the relation between the compressive and tensile stiffness of bilinear spring and the asymmetric arrangements of bilinearity strongly influence the dynamic behavior, which can also help us understand the simulation results in current 2D case.

Figure 7 shows the propagation of a single-cycle incident wave in a spring—mass chain system from the opposite directions. Two types of pulses are formed when the incidence enters the bilinear section; a dashed line divides a pulse into different parts each of which relates to bilinear springs in the same state, compression or tension. Therefore, TC pulse (CT pulse) indicates a pulse with a tensile zone followed by a compressive zone (a compressive zone is followed by a tensile zone) [15].

Since a tensile wave travels with a higher speed than a compressive one under current stiffness setup ( $\kappa_c$   $\nearrow \ll \kappa_t$   $\nearrow$ ), we expect an increase in distance between the tensile and compressive zones and the generation of a zero deformation zone (the horizontal region with nearly constant positive displacement) for a TC pulse; in terms of a CT pulse, we expect that the faster tensile wave front catches up with the slower compressive one and then changes the pulse type to TC one. Table 3 concludes these two processes.



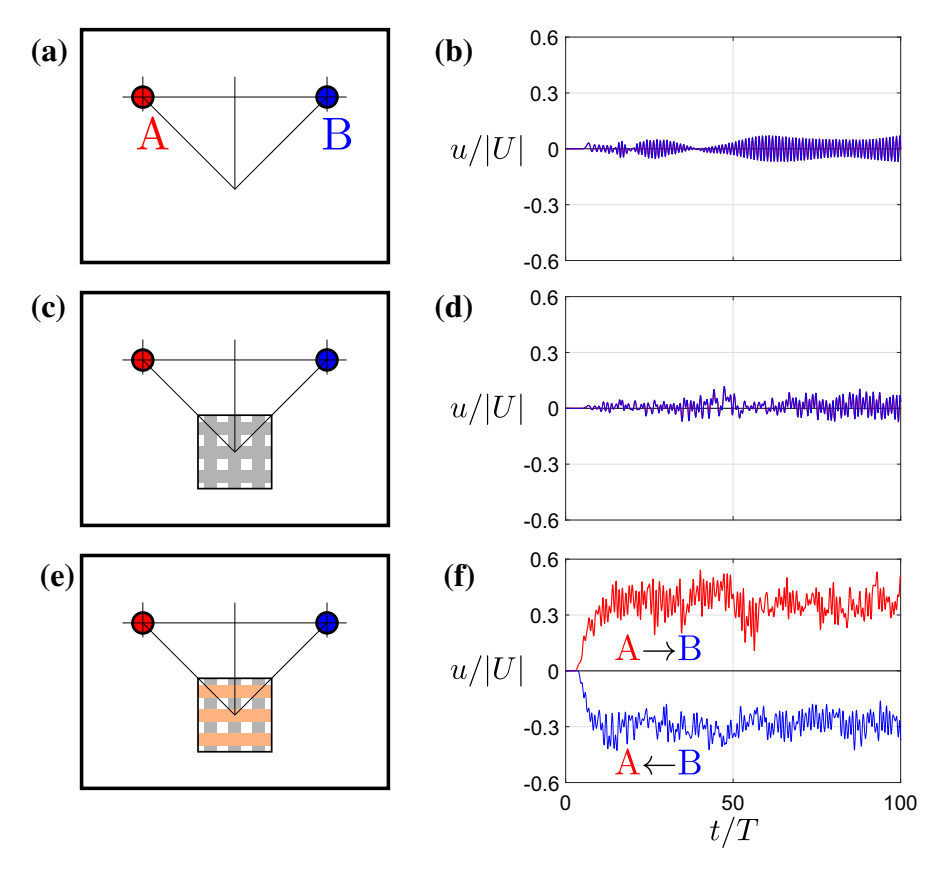


Fig. 6 Simulation results. The left column depicts three different simulation setups, refer to Figs. 4 and  $5(\mathbf{b})$ ; the right one records the corresponding dynamic profiles of receivers, the normalized displacement u/|U| against the number of excitation period. **a** shows the pure linear setup, and **b** shows its reciprocal results with the overlapping low-amplitude dynamic profiles. The setup in **c** contains a squared section with the bilinearity in

both horizontal and vertical directions; the overlapping dynamic results in  $(\mathbf{d})$  again indicate the reciprocity. Spatial asymmetry is introduced in  $(\mathbf{e})$ , and the combination of bilinearity and spatial asymmetry is arranged in horizontal direction only;  $\mathbf{f}$  shows that the dynamic profiles of receivers have the opposite signs of steady shifts with positive one for the source located at position A and negative one at B

Table 3 Explanation of nonreciprocal wave propagation in an asymmetric bilinear chain

Pulse Type	Property	Stiffness	Wave Speed	Result
TC pulse	Tens. zone precedes Comp. zone			TC pulse with zero deformation zone
CT pulse	Comp. zone precedes Tens. zone	$\kappa_{c} \nearrow \ll \kappa_{t} \nearrow$	Comp. wave ≪ Tens. wave	TC pulse

In the current 2D monatomic lattice, an incident wave is generated by a continuous excitation in the linear section. Upon entering the nonlinear section consisting of multiple asymmetric bilinear chains connected together, the incidence is best thought of as a

string of multiple cycles of two types of pulses, TC and CT one, see Table 3. After having the similar propagation process shown in Fig. 7, the transmitted wave with single sign then scatters into the linear section again and is detected by the receiver. For example, as the



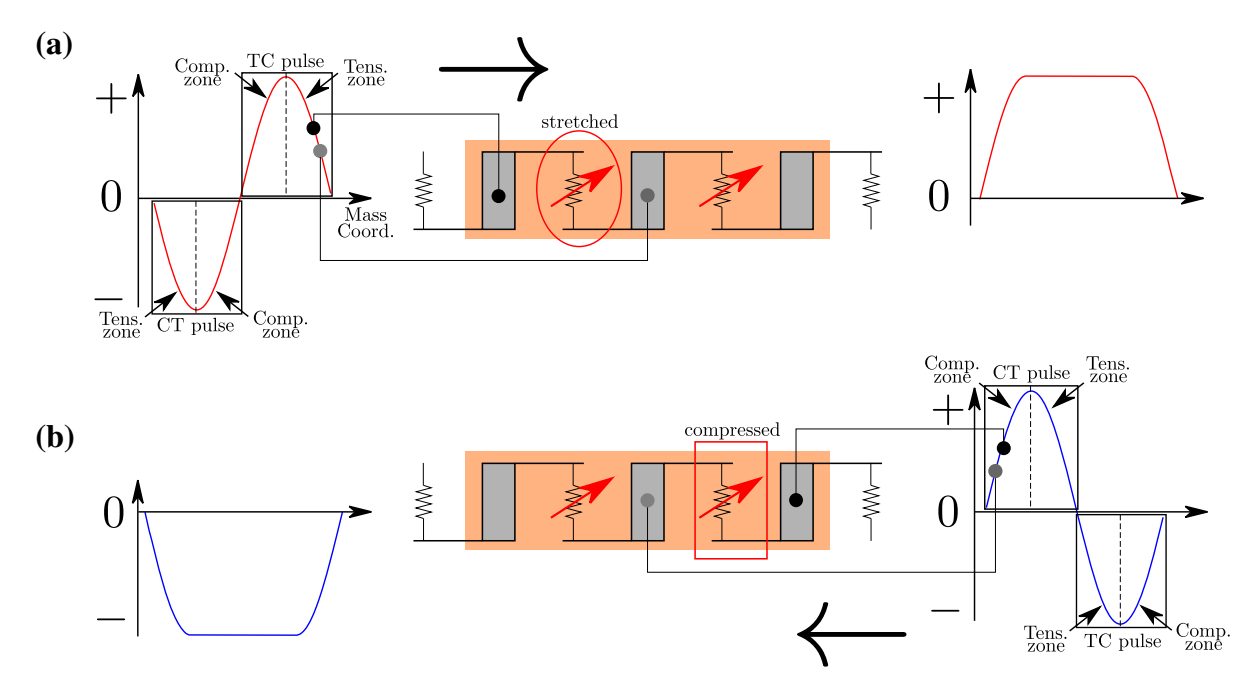


**Fig. 7** Nonreciprocal wave propagation in an asymmetric bilinear chain. **a** and **b** show the single-cycle incident waves and the transmitted waves for incidence from left and right, respectively.

The chains in shade areas contain structurally asymmetric unit cells connected by identical bilinear springs, see Fig. 4f

nonreciprocal case in Fig. 6(e) shows, the same stimulus generates incident waves coming from opposite directions with reversed order of pulse types, resulting in transmitted pulses of the same pulse type but with oppositely signed displacement: the incident wavefield from position A on the left experience the same situation as Fig. 7(a) describes, and Fig. 7(b) represents the transmission of the same incidence from B on the right.

#### 4.5 Amplitude independence

The nonreciprocal phenomenon of the opposite-sign dynamic profiles is presumably independent of input excitation amplitude given that the bilinear springs in the 2D lattice are only sensitive to the sign of the relative wave motion between unit cells connected to them. Here, we apply the continuous excitation with several different amplitudes to show the amplitude-independent property.

We first set excitation amplitude positive, U>0, as we did in previous demonstrations. Figure 8a shows that the resultant dynamic profile scales linearly with

the input amplitude, so that the normalized results overlap and therefore amplitude independence holds. Setting the excitation amplitude negative, U < 0, shows the same scaling and amplitude independence, see Fig. 8b; however, the dynamic profiles are different from those of positive U. The reason is that the opposite signs of excitation amplitudes lead to different pulse type orders within each cycle of the incident wave: A CT pulse precedes a TC one for the negative-value case; the reverse condition, TC before CT, is the case of positive excitation amplitude. Since they are fundamentally different inputs, this phenomenon does not violate the amplitude-independent property.

#### 4.6 Alternative modulation arrangements

We display two more nonreciprocal demonstrations applying different linear and nonlinear section setups to show the micro-modulation design's capability of breaking reciprocity.

Bilinearity + spatial asymmetry in both horizontal and vertical directions. Here, we arrange the combination of bilinearity and spatial asymmetry in both



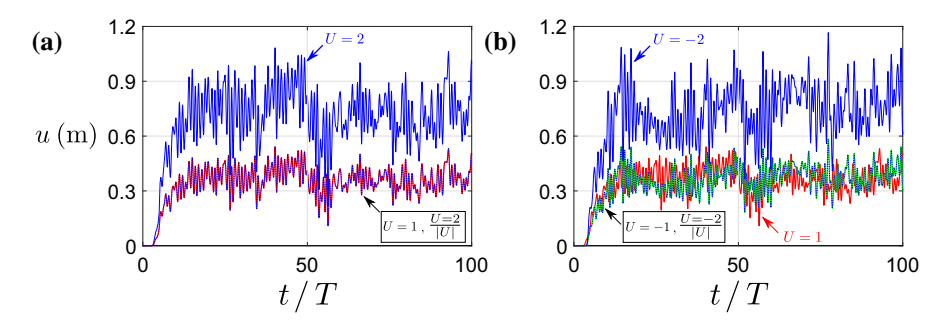


Fig. 8 Amplitude independence. Simulations are performed in the setup with asymmetric bilinear arrangement along horizontal direction only in the nonlinear section, refer to Fig. 6e, and the dynamic profiles of receiver at position B are recorded. a shows the results when we set positive excitation amplitudes U = 1 and 2 m, see Eq. (13); the overlapping normalized results

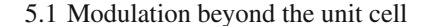
demonstrate the amplitude-independent property. **b** shows the results with amplitudes  $U=\pm 1$  and -2 m; the normalization of all negative-amplitude profiles is overlapped; however, because changing the sign of amplitude results in a different incident wave, the opposite signs of excitation amplitudes demonstrate different normalized dynamic behaviors

horizontal and vertical directions and set the positions for locating source and receiver which are A, B and C as Fig. 9a shows. Dynamic profiles with the opposite amplitudes can be observed when considering the positions A and B, but the amplitude of the negative profile decreases approaching to zero, see Fig. 9b. For case of considering positions B and C where the receiver can presumably detect the signal coming from the source in linear condition, we can also obtain the dynamic profiles with opposite shifts as Fig. 9c shows.

**Broadband effect.** Our nonreciprocal design works for any case of the receiver being located in the propagation-free region relative to the source. Here, we set  $\kappa_1=1$  N/m,  $\kappa_2=1.5$  N/m for linear springs and keep the nonlinear section and excitation unchanged, which results in a directional wave propagation with ranges  $\theta_{\rm range}\approx 102^{\circ}$  instead of several discrete directions in previous demonstrations, see Fig. 10a and b. As Fig. 10c shows, we can still get the nonreciprocal dynamic profiles with the opposite signs before and after interchanging the positions of source and receiver.

## 5 Macro-modulation: spatial asymmetry of bilinear section

Micro-modulation within the unit cell is a fundamental way of generating spatial asymmetry. With the source and receiver locations fixed, the whole bilinear section can be modulated in its entirety to further generate additional spatial asymmetry.



In addition to generating the spatial asymmetry within the unit cell, we can extend the spatial modulation at a larger scale. When the positions of source and receiver are fixed, the modification of the whole bilinear section in its entirety can generate additional spatial asymmetry in a macro-perspective. However, simply performing the macro-modulation for the whole bilinear section without the micro-modulation in its unit cells is proved to be an inefficient way of breaking reciprocity: It is shown in Appendix B that spatial asymmetry introduced by macro-modulation alone gives very little non-reciprocity. Adding additional macro-modulation of spatial asymmetry into the spatially micro-modulated bilinear section is able to adjust the original nonreciprocal results.

Here, we use the demonstrated nonreciprocal case of bilinearity and spatial asymmetry existing in both horizontal and vertical directions, see Fig. 9 in Sect. 4, and introduce additional macro-modulations of spatial asymmetry in the whole bilinear section to check their influences on nonreciprocity. We only take the positions A and B for tests, and the same excitation is applied, see Eq. (13).

#### 5.2 Horizontal translation

We fix the positions of source and receiver, but displace the whole bilinear section laterally by  $\Delta N$  number of springs from its original position, as Fig. 11a shows.



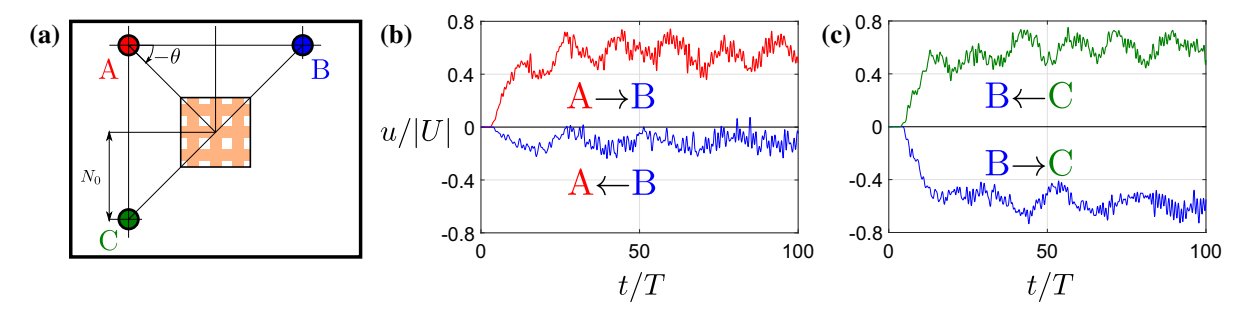


**Fig. 9** Bilinearity + spatial asymmetry in both horizontal and vertical directions. **a** shows the simulation setup. The combination of bilinearity and spatial asymmetry is arranged in both horizontal and vertical directions. Three positions A, B and C are used to locate source and receiver;  $N_0 = 10$  for position

C. **b** depicts the different dynamic behaviors with decreasing negative shift for incidence from position B compared with Fig. 6f. **c** shows the dynamic profiles with the opposite signs when positions B and C are considered

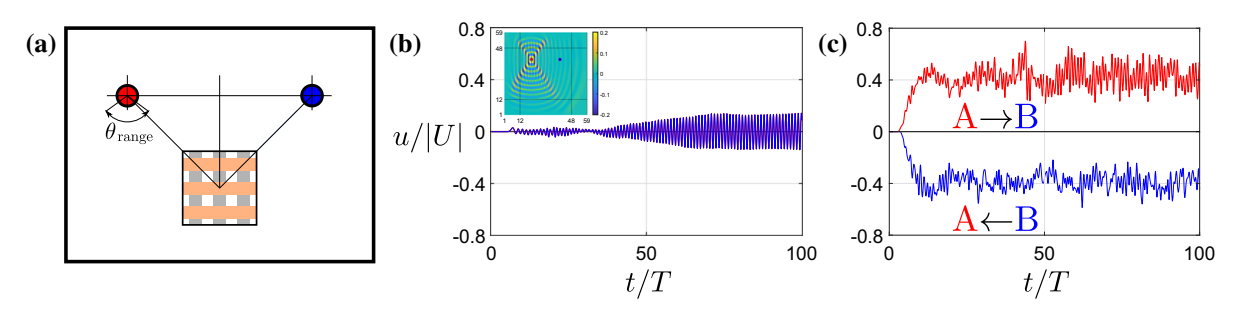


Fig. 10 Broadband effect. a shows the directional wave propagation covering a range with  $\theta_{\rm range} \approx 102^{\circ}$ . b shows the dynamic profiles in the reciprocal linear case; the insert plot intuitively depicts the propagating ranges. c shows the nonre-

ciprocal dynamic behaviors with the opposite signs of displacements before and after interchanging the positions of source and receiver

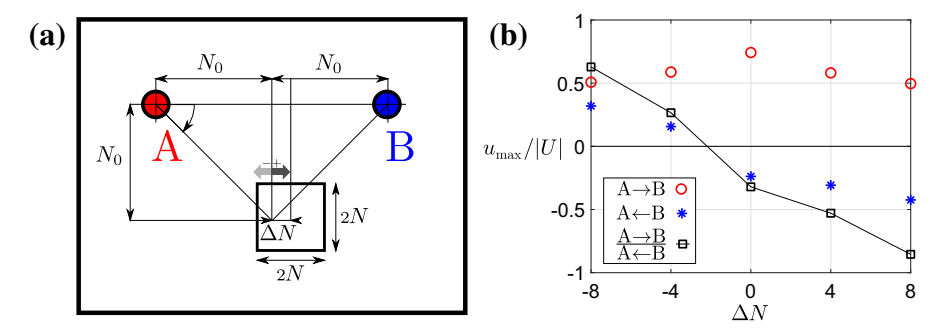


Fig. 11 Horizontal translation. **a** shows the horizontal translation of the bilinear section from its original position with positive  $\Delta N$  the distance (number of springs) moved to the right;  $N_0 = 10$ , N = 8. **b** denotes the effect that value  $\Delta N$  has on non-reciprocal behavior, which is indicated by the maximum ampli-

tudes of dynamic profiles at two receivers and the ratio between them; the right translation results in the ratio approaching to -1, meaning the exaggeration of nonreciprocity; and the left one leads to the same amplitude sign, weakening the nonreciprocity



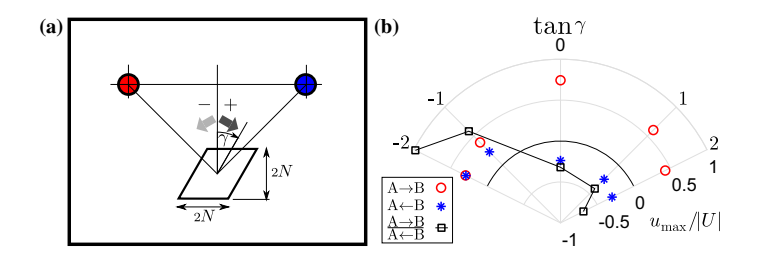


Fig. 12 Shape deformation. a depicts the shape deformation of the bilinear section into a parallelogram with vertical boundaries tilted clockwise by positive angle  $\gamma$ ; this demonstration uses the same parameters as that in Fig. 11(a). b denotes the influence of tilting angle  $\gamma$ , labeled by  $\tan \gamma$  in the polar plot; the maximum

amplitudes of dynamic profiles at two receivers and their ratio for each value of  $\gamma$  are used for checking the effect of adjustment; and the modulations of the bilinear section can either weaken (counterclockwise tilting) or exaggerate (clockwise tilting) the nonreciprocity

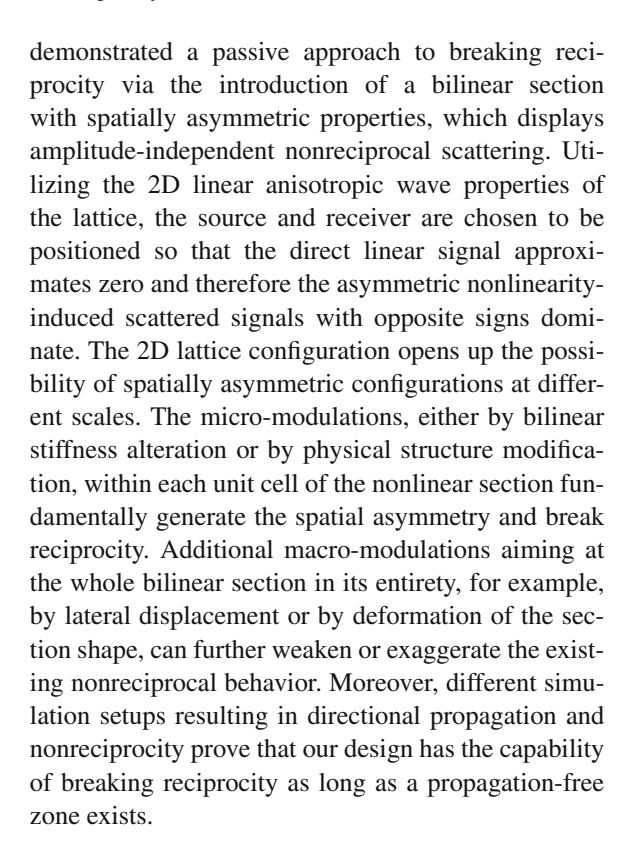
Simulation results are presented in Fig. 11b; instead of the whole dynamic profiles, only the maximum amplitudes are recorded; and the ratios of two maximum amplitudes before and after interchanging the positions of source and receiver for each value of  $\Delta N$  are also calculated, cases closer to -1 being treated as the more significantly nonreciprocal results. The lateral translation to the left,  $\Delta N < 0$ , results in two dynamic profiles with the same positive sign and the amplitude ratio approaching to +1, weakening the nonreciprocal behavior. See Appendix B for an explanation of this phenomenon.

#### 5.3 Shape deformation

Another macro-modulation fixes the center of the bilinear section at its original position and deforms its previous square shape into a parallelogram. In Fig. 12a,  $\gamma$  describes the angle by which the vertical boundaries of the bilinear section tilt. Namely, we displace the bilinear arrangements laterally by  $n \tan \gamma$ , n=1,2,...,N from the center of bilinear section to the top for the upper half, and  $-n \tan \gamma$  from the center to the bottom for the lower half. Figure 12b depicts the effect of the shape modulation, showing that the clockwise tilt,  $\gamma$  or  $\tan \gamma > 0$ , exaggerates the nonreciprocal behavior, but counterclockwise one,  $\gamma$  or  $\tan \gamma < 0$ , weakens the nonreciprocity. We refer to Appendix B for an explanation of this phenomenon.

#### 6 Conclusion

Taking advantage of the directional nature of wave propagation in the 2D monatomic lattice, we have



**Acknowledgements** This work is supported by the NSF EFRI Program under Award No. 1641078.

**Data availability** Simulation data were generated by ODE solver in MATLAB. The datasets generated during and/or analyzed during the current study are available from the corresponding author on reasonable request.

#### **Declarations**

Conflict of Interest The authors declare that they have no conflict of interest.



#### Appendix A: Perfectly matched layers

To simulate a nonreflecting infinite transverse wave, perfectly matched layers (PMLs) are attached to the sides and corners of the 2D monatomic lattice, as Fig. 13 shows. The PML is a damped monatomic lattice with ramped-up damping coefficients to avoid reflections caused at the interfere of damped and non-damped sections. The varying damping coefficients can be expressed as

$$C_j = C_{max} \left(\frac{j}{N_{PML}}\right)^3,\tag{A1}$$

where  $C_j$  represents the damping coefficient at index j that starts from 1 at the interfere of PML and non-damped lattice,  $C_{max}$  is the maximum damping coefficient located at the end of the PML, and  $N_{PML}$  denotes the number of dampers per column for the upper and lower PMLs or per row for the left and right PMLs in Fig. 13. The damping coefficients in PMLs at four corners are more complicated to be expressed but also obey the rule of values increasing from interfere to boundaries. Here, we take  $N_{PML}=10$  and  $C_{max}=10$  kg·s<sup>-1</sup> for all numerical simulations in this paper.

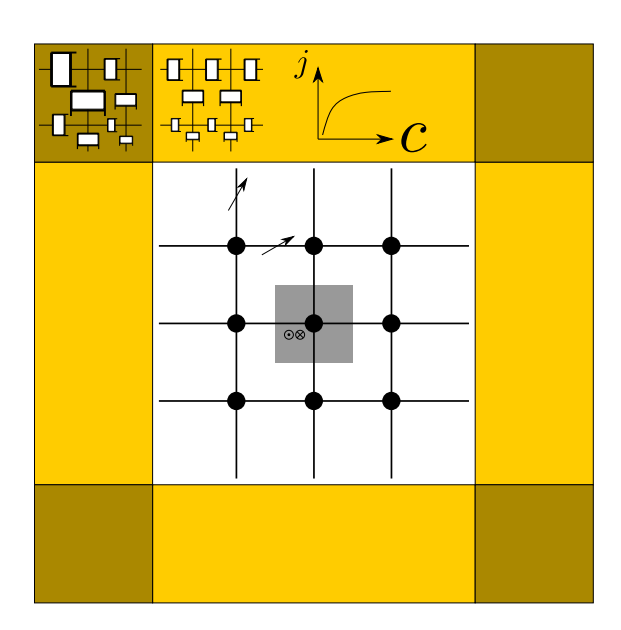


Fig. 13 Perfectly matched layers (PMLs) surround the 2D monatomic lattice. PML is a damped monatomic lattice with damping coefficients ramping up from the interfere of damped and nondamped lattice to the boundary. The size of damping cartoon in PMLs denotes the value of damping coefficient; the larger the size, the greater the value

# Appendix B: Spatial distribution of nonreciprocal wavefield

Here, we qualitatively explain some phenomena using simulation results of wave propagation for various configurations illustrated in Fig. 14; for each configuration, the left wavefield depicts the source at A on the left and the right one has source on the right at B.

Figure 14a shows a reciprocal case with different linear stiffness values inside and outside the square section. Bilinearity is introduced to the square section without any type of spatial asymmetry in (b), and reciprocity is maintained. Two time-responsive dynamic profiles in the top row confirm the reciprocity. (a) and (b) together illustrate that only the reflection occurs when stiffness mismatch exists, and that spatial asymmetry is a necessary ingredient of breaking reciprocity.

When the horizontally arranged micro-modulation of spatial asymmetry is introduced to the nonlinear section as Fig. 14c depicts, directional scattering with opposite signs of displacements at left and right side of square section indicates a significant degree of nonreciprocity. As comparison, (d) and (e) show that bilinearity plus macro-modulation of spatial asymmetry alone cannot generate the similar level of nonreciprocity apart from some reflections, which also indicates that only micro-modulation can efficiently generate significantly nonreciprocal results.

However, macro-modulation can effectively adjust the nonreciprocity caused by micro-modulation. Figure 14g-j demonstrates several adjustments of two macromodulations to the nonreciprocal results in configuration (f) within which the combination of bilinearity and micro-modulated spatial asymmetry is arranged in both horizontal and vertical directions inside the square section. The scattering region, which contains masses with single-sign displacements, covers certain parts around the nonlinear section; e.g., in (f), the scattering region with positive sign appears around the top right corner and the negative one is around the bottom left corner. When we perform the additional macro-modulations, the scattering regions can move accordingly, resulting in the different dynamic responses collected at the fixed receivers. As (g) shows, the horizontal translation of nonlinear section to the left shifts the scattering regions to the left as well, changing the original opposite signs of displacements to the merely positive results regardless of where the incidence comes from and therefore weakens the original nonreciprocal



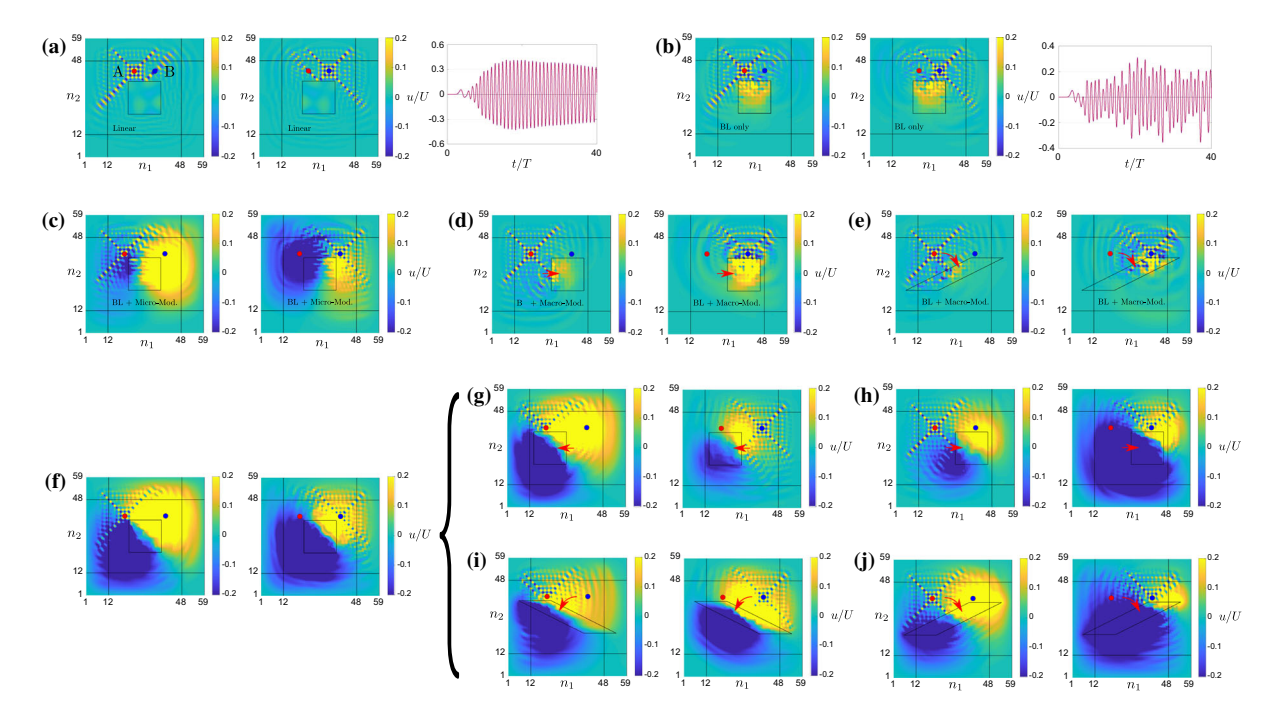


Fig. 14 Spatial distribution of wavefield for a variety of configurations. In each case, the plot on the left (right) is for the source at A (B). a shows a reciprocal case with different but still linear stiffness inside the square section; reciprocity is confirmed by the identical signals. b is also reciprocal with bilinearity in the square section but with no spatial asymmetry, confirming the condition of reciprocity. c depicts the case of bilinearity plus micro-modulation of spatial asymmetry in horizontal direction. It leads to a significant nonreciprocity as shown by the directional

scattering with opposite signs of displacements . As compared to  $\mathbf{c}$ , cases  $\mathbf{d}$  and  $\mathbf{e}$  demonstrate relatively small nonreciprocity in the presence of bilinearity and two types of macro-modulation, translation and deformation, respectively.  $\mathbf{f}$  is another nonreciprocal case with micro-modulation arranged in both horizontal and vertical directions. Additional macro-modulations, horizontal translation with  $\Delta N = \mp 8$  in  $(\mathbf{g})$  and  $(\mathbf{h})$  and shape deformation with tan  $\gamma = \mp 2$  in  $(\mathbf{i})$  and  $(\mathbf{j})$  illustrate a variety of adjustments to the original nonreciprocal configuration in  $(\mathbf{f})$ 

results. The translation to the right, see (h), causes the scattering regions move to the right and maximizes the difference between displacements with opposite signs obtained at receivers, leading to the exaggeration of the original nonreciprocity. Similar behaviors are obtained for a counterclockwise tilt of the nonlinear section in (i) and clockwise tilt in (j).

#### References

- Nassar, H., Yousefzadeh, B., Fleury, R., Ruzzene, M., Alú, A., Daraio, C., Norris, A.N., Huang, G., Haberman, M. R.: Nonreciprocity in acoustic and elastic materials. Nat. Rev. Mater. 5(9), 667–685 (2020)
- Fleury, R., Sounas, D.L., Sieck, C.F., Haberman, M.R., Alú, A.: Sound isolation and giant linear nonreciprocity in a compact acoustic circulator. Science 343(6170), 516–519 (2014)
- Zangeneh-Nejad, F., Fleury, R.: Doppler-based acoustic gyrator. Appl. Sci. 8(7), 1083 (2018)

- Trainiti, G., Ruzzene, M.: Non-reciprocal elastic wave propagation in spatiotemporal periodic structures. New J. Phys. 18(8), 082047 (2016)
- Nassar, H., Chen, H., Norris, A.N., Haberman, M.R., Huang, G.L.: Non-reciprocal wave propagation in modulated elastic metamaterials. Proc. Royal Soc. A Mathe-matical Phys. Eng. Sci. 473(2202), 20170188 (2017)
- Nassar, H., Chen, H., Norris, A.N., Huang, G.L.: Nonreciprocal flexural wave propagation in a modulated metabeam. Extreme Mech. Letts. 15, 97–102 (2017)
- Nassar, H., Xu, X.C., Norris, A.N., Huang, G.L.: Modulated phononic crystals: non-reciprocal wave propagation and Willis materials. J. Mech. Phys. Solids 101, 10–29 (2017)
- 8. Wang, Y., Yousefzadeh, B., Chen, H., Nassar, H., Huang, G., Daraio C.: Observation of nonreciprocal wave propagation in a dynamic phononic lattice. *Phys. Rev. Letts.* **2018**, 121(19)
- Goldsberry, B.M., Wallen, S.P., Haberman, M.R.: Non-reciprocal wavepropagation in mechanically-modulated continuous elastic metamaterials. J. Acoustical Soc. Am. 146(1), 782–788 (2019)



- Goldsberry, B.M., Wallen, S.P., Haberman M.R.: Nonreciprocal vibra-tions of finite elastic structures with spatiotem-porally modulated material properties. *Phys. Rev. B2020*, 102(1)
- Wallen, S. P., Haberman, M. R., Lu, Z., Norris, A., Wiest, T., Seepersad, C. C.: Static and dynamic non-reciprocity in bilinear structures. *In Proceedings of Meetings on Acoustics* 21ISNA, 2018, Acoustical Society of America
- Grinberg, I., Vakakis, A.F., Gendelman, Oleg V.: Acoustic diode: wave non-reciprocity in nonlinearly coupled waveguides. Wave Motion 83, 49–66 (2018)
- Moore, K. J., Bunyan, J., Tawfick, S., Gendelman, O. V., Li, S., Leamy, M., Vakakis, A. F.: Nonreciprocity in the dynamics of coupled oscillators with nonlinearity, asymmetry, and scale hierarchy. *Phys. Rev. E2018*, 97(1)
- Zhang, Q., Li, W., Lambros, J., Bergman, L. A., Vakakis, A. F.: Pulse transmission and acoustic non-reciprocity in a granular channel with symmetry-breaking clearances. *Granular Matter*, 2019, 22(1)
- Lu, Z., Norris, A. N.: Non-reciprocal wave transmission in a bilinear spring-mass system. J. Vib. Acoust. 2019, 142(2)
- Zhaocheng, Lu., Norris, Andrew N.: Unilateral and nonreciprocal transmission through bilinear spring systems. Extreme Mech. Letts. 42, 101087 (2021)
- Fang, L., Mojahed, A., Darabi, A., Vakakis, A. F., Leamy, M. J.: Passive nonreciprocity in a system of asymmetrical rotational oscillators. *Phys. Rev. Appl.* 2021, 15(3)
- Darabi, A., Fang, L., Mojahed, A., Fronk, M. D., Vakakis, A. F., Leamy, M. J.: Broadband passive nonlinear acoustic diode. *Phys. Rev. B*, 2019, 99(21)

- Nash, L.M., Kleckner, D., Read, A., Vitelli, V., Turner, A.M., Irvine, W.T.M.: Topological mechanics of gyroscopic metamaterials. Proc. National Acad. Sci. 112(47), 14495–14500 (2015)
- Khanikaev, A. B., Fleury, R., Mousavi, S. H., Alú, A.: Topologically robust sound propagation in an angular-momentum-biased graphene-like resonator lattice. *Nature Commun.* 2015, 6(1)
- Wang, P., Lu, L., Bertoldi, K.: Topological phononic crystals with one-way elastic edge waves. *Phys. Rev. Letts*. 2015, 115(10)
- Qian, W., Chen, H., Nassar, H., Huang, G.: Non-reciprocal rayleigh wave propagation in space-time modulated surface.
   J. Mech. Phys. Solids 146, 104196 (2021)
- Ruzzene, Massimo, Scarpa, Fabrizio, Soranna, Francesco: Wave beaming effects in two-dimensional cellular structures. Smart Mater. Struct. 12(3), 363–372 (2003)
- Spadoni, A., Ruzzene, M., Gonella, S., Scarpa, F.: Phononic properties of hexagonal chiral lattices. Wave Motion 46(7), 435–450 (2009)
- Narisetti, R. K., Ruzzene, M., Leamy, M. J.: A perturbation approach for analyzing dispersion and group velocities in two-dimensional nonlinear periodic lattices. *J. Vib. Acoust.* 2011, 133(6)

**Publisher's Note** Springer Nature remains neutral with regard to jurisdictional claims in published maps and institutional affiliations.

